# Quality factor of Si-based photonic crystal L3 nanocavities probed with an internal source

**M. El Kurdi**[1]**, X. Checoury**[1]**, S. David**[1]**, T. P. Ngo**[1]**, N. Zerounian**[1]**, P. Boucaud**[1]***, O. Kermarrec**[2]**, Y. Campidelli**[2]**, D. Bensahel**[2]

[1] *Institut d'Electronique Fondamentale, CNRS Univ Paris Sud, Btiment 220, F-91405 Orsay Cedex, France*

[2] *STMicroelectronics, 850 rue Jean Monnet, F-38920 Crolles, France*
*\* Corresponding author : philippe.boucaud@ief.u-psud.fr*

*http://pages.ief.u-psud.fr/QDgroup/index.html*

**Abstract:** We have investigated the quality factors of silicon-based photonic crystal nanocavities using the photoluminescence of a single layer of Ge/Si self-assembled islands as an internal source. We focus on membrane-type L3 elongated cavities with or without their lateral edge air holes shifted in position. The photoluminescence measurements are performed at room temperature. We show that the quality factor of the fundamental mode observed at a normalized frequency $u = a/\lambda \simeq 0.25$ is strongly dependent on the incident pump power. This dependence is associated with the free-carrier absorption of the photogenerated carriers. The slope of the quality factor *vs.* incident pump power gives access to the carrier recombination dynamics in these Si-based nanocavities. The measurements indicate that the carrier dynamics is controlled by non-radiative recombination associated with surface recombinations. A surface recombination velocity of $4.8 \times 10^4$ *cm/s* is deduced from the experiments. The spectral red-shift of the cavity modes as a function of incident pump power is correlated to the temperature rise due to thermo-optic effects. The measured temperature rise, which can reach 190 K, is correlated to the value estimated by a thermal analysis.

© 2008 Optical Society of America

**OCIS codes:** (230.0230) Optical devices - (230.5298) photonic crystals

---

## References and links

1. J. M. Gerard, B. Sermage, B. Gayral, B. Legrand, E. Costard, and V. Thierry-Mieg, "Enhanced spontaneous emission by quantum boxes in a monolithic optical microcavity," Phys. Rev. Lett. **81**, 1110–1113 (1998).
2. T. Yoshie, A. Scherer, J. Hendrickson, G. Khitrova, H. M. Gibbs, G. Rupper, C. Ell, O. B. Shchekin, and D. G. Deppe, "Vacuum Rabi splitting with a single quantum dot in a photonic crystal nanocavity," Nature **432**, 200–203 (2004).
3. Y. Akahane, T. Asano, B. S. Song, and S. Noda, "High-Q photonic nanocavity in a two-dimensional photonic crystal," Nature **425**, 944–947 (2003).
4. D. Englund, I. Fushman, and J. Vuckovic, "General recipe for designing photonic crystal cavities," Opt. Express **13**, 5961–5975 (2005).
5. B. S. Song, S. Noda, T. Asano, and Y. Akahane, "Ultra-high-Q photonic double-heterostructure nanocavity," Nature Materials **4**, 207–210 (2005).

6. T. Asano, B. S. Song, Y. Akahane, and S. Noda, "Ultrahigh-Q nanocavities in two-dimensional photonic crystal slabs," IEEE J. Sel. Top. Quantum Electron. **12**, 1123–1134 (2006).
7. T. Tanabe, M. Notomi, E. Kuramochi, A. Shinya, and H. Taniyama, "Trapping and delaying photons for one nanosecond in an ultrasmall high-Q photonic-crystal nanocavity," Nat. Photonics **1**, 49–52 (2007).
8. E. Weidner, S. Combrie, N. V. Q. Tran, A. De Rossi, J. Nagle, S. Cassette, A. Talneau, and H. Benisty, "Achievement of ultrahigh quality factors in GaAs photonic crystal membrane nanocavity," Appl. Phys. Lett. **89**, 221104 (2006).
9. P. E. Barclay, K. Srinivasan, and O. Painter, "Nonlinear response of silicon photonic crystal microresonators excited via an integrated waveguide and fiber taper," Opt. Express **13**, 801–820 (2005).
10. D. Labilloy, H. Benisty, C. Weisbuch, C. J. M. Smith, T. F. Krauss, R. Houdre, and U. Oesterle, "Finely resolved transmission spectra and band structure of two-dimensional photonic crystals using emission from InAs quantum dots," Phys. Rev. B **59**, 1649–1652 (1999).
11. S. David, M. El kurdi, P. Boucaud, A. Chelnokov, V. Le Thanh, D. Bouchier, and J. M. Lourtioz, "Two-dimensional photonic crystals with Ge/Si self-assembled islands," Appl. Phys. Lett. **83**, 2509–2511 (2003).
12. X. Li, P. Boucaud, X. Checoury, O. Kermarrec, Y. Campidelli, and D. Bensahel, "Probing photonic crystals on silicon-on-insulator with Ge/Si self-assembled islands as an internal source," J. Appl. Phys. **99**, 023103 (2006).
13. X. Li, P. Boucaud, X. Checoury, M. El Kurdi, S. David, S. Sauvage, N. Yam, F. Fossard, D. Bouchier, J. M. Fedeli, A. Salomon, V. Calvo, and E. Hadji, "Quality factor control of Si-based two-dimensional photonic crystals with a Bragg mirror," Appl. Phys. Lett. **88**, 091122 (2006).
14. J. S. Xia, Y. Ikegami, Y. Shiraki, N. Usami, and Y. Nakata, "Strong resonant luminescence from Ge quantum dots in photonic crystal microcavity at room temperature," Appl. Phys. Lett. **89**, 201102 (2006).
15. J. Hendrickson, B. C. Richards, J. Sweet, S. Mosor, C. Christenson, D. Lam, G. Khitrova, H. M. Gibbs, T. Yoshie, A. Scherer, O. B. Shchekin, and D. G. Deppe, "Quantum dot photonic-crystal-slab nanocavities: Quality factors and lasing," Phys. Rev. B **72**, 193303 (2005).
16. J. Vuckovic, M. Loncar, H. Mabuchi, and A. Scherer, "Optimization of the Q factor in photonic crystal microcavities," IEEE J. Quantum Electron. **38**, 850–856 (2002).
17. A. R. A. Chalcraft, S. Lam, D. O'Brien, T. F. Krauss, M. Sahin, D. Szymanski, D. Sanvitto, R. Oulton, M. S. Skolnick, A. M. Fox, D. M. Whittaker, H. Y. Liu, and M. Hopkinson, "Mode structure of the L3 photonic crystal cavity," Appl. Phys. Lett. **90**, 241117 (2007).
18. S. Fan, P. R. Villeneuve, J. D. Joannopoulos, and E. F. Schubert, "High extraction efficiency of spontaneous emission from slabs of photonic crystals," Phys. Rev. Lett. **78**, 3294–3297 (1997).
19. P. Boucaud, S. Sauvage, M. Elkurdi, E. Mercier, T. Brunhes, V. Le Thanh, D. Bouchier, O. Kermarrec, Y. Campidelli, and D. Bensahel, "Optical recombination from excited states in Ge/Si self-assembled quantum dots," Phys. Rev. B **64**, 155310 (2001).
20. T. D. Happ, I. I. Tartakovskii, V. D. Kulakovskii, J. P. Reithmaier, M. Kamp, and A. Forchel, "Enhanced light emission of InxGa1-xAs quantum dots in a two-dimensional photonic-crystal defect microcavity," Phys. Rev. B **66**, 041303 (2002).
21. R. A. Soref and B. R. Bennett, "Electrooptical effects in silicon," IEEE J. Quantum Electron. **23**, 123–129 (1987).
22. A. J. Sabbah and D. M. Riffe, "Measurement of silicon surface recombination velocity using ultrafast pump-probe reflectivity in the near infrared," J. Appl. Phys. **88**, 6954–6956 (2000).
23. G. Cocorullo, F. G. Della Corte, and I. Rendina, "Temperature dependence of the thermo-optic coefficient in crystalline silicon between room temperature and 550 K at the wavelength of 1523 nm," Appl. Phys. Lett. **74**, 3338–3340 (1999).
24. A. D. McConnell and K. E. Goodson, "Thermal conduction in silicon micro- and nanostructures," Annual review of heat transfer **14**, 129–168 (2005).
25. G. E. Jellison and F. A. Modine, "Optical-absorption of silicon between 1.6-Ev and 4.7-Ev at elevated-temperatures," Appl. Phys. Lett. **41**, 180–182 (1982).
26. T. Trupke, M. A. Green, P. Wurfel, P. P. Altermatt, A. Wang, J. Zhao, and R. Corkish, "Temperature dependence of the radiative recombination coefficient of intrinsic crystalline silicon," J. Appl. Phys. **94**, 4930–4937 (2003).
27. J. Dziewior and W. Schmid, "Auger coefficients for highly doped and highly excited silicon," Appl. Phys. Lett. **31**, 346–348 (1977).

## 1.  Introduction

One of the most interesting feature of two-dimensional photonic crystals is their ability to provide cavities with high quality factors (Q) and very small modal volumes (V) opening the route to solid-state cavity quantum electrodynamic measurements. For a single emitter in a nanocavity with a large Q/V factor, the recombination rate can be enhanced by the Purcell effect. It leads to a better coupling of the spontaneous emission to a single cavity mode and a larger radiation efficiency [1]. Strong coupling regime between a dipole emitter and an electromagnetic mode

has even been observed with photonic crystal nanocavities [2]. Apart from their application in active devices like e.g. single photon emitters, nanolasers with reduced thresholds and large coupling factor $\beta$ values, nanocavities with very large quality factors can be used in different kinds of high resolution sensors or filters or non linear optical components.

Several methods have been proposed over the past years to design and realize two-dimensional photonic crystals with high quality factors and reduced mode volumes. It requires to control out-of-plane losses which is particularly difficult with small mode volumes. A major step was achieved by Akahane *et al.* [3] who did demonstrate the suppression of radiation losses by minimizing the components of the Fourier transform of the electromagnetic field within the light cone. This can be achieved by avoiding abrupt changes in the envelope of the cavity mode field. One possibility for this gentle confinement of the electromagnetic field relies on shifting the edge air holes of photonic crystal cavities by a fraction of the lattice parameter. For a membrane-type L3 elongated cavity, which consits of a line with three holes missing, this approach can lead to quality factors up to 100 000. Starting from an inverse point of view, the engineering of modal k-space field distribution of the cavity modes was further optimized by Englund *et al.*, who proposed to shift not only the edge air holes but also the nearest neighbors to obtain a sinc law for the mode field envelope [4]. By this method, the components of the Fourier transform of the electromagnetic field within the light cone are expected to be dramatically suppressed, leading to predicted very high quality factors up to $4 \times 10^6$. Another approach to achieve very high quality factors relies on the use of photonic heterostructures or multi-step heterostructures, i.e. by locally changing the lattice parameter of a waveguide photonic crystal [5]. Quality factors up to 1 million have been achieved by this method [6]. An alternative approach was proposed by Kuramochi *et al.*, by changing locally the lateral width of a line defect. An experimental loaded Q-value of $1.2 \times 10^6$ was reported for a width-modulated waveguide by these authors [7].

The measurement of very high quality factor remains a difficult task, since one has to disentangle the contribution from the intrinsic value of the quality factor from the contribution associated with the measurement. One way to measure the quality factor of a nanocavity is to couple the cavity with a lateral waveguide. This technique has been extensively used to characterize different types of cavities using a tunable external cavity laser diode. The quality factor is in this case dependent on the lateral coupling of the waveguide, the quality factor being obtained by the linewidth of the decreased transmission of the waveguide or by the linewidth of the radiation spectrum of the cavity. The coupling between the cavity and the side waveguide needs to be taken into account to extract the intrinsic value of quality factor since one measures the quality factor loaded by the excitation waveguide [8]. In a similar way, a method based on the evanescent coupling of a tapered optical fiber has been proposed by Barclay and coworkers [9]. In the latter case, the measured value of the quality factor also depends on the strength of the coupling. Another approach to characterize cavity modes is to rely on an internal source which can be optically or electrically excited. The internal source can be either semiconductor quantum wells or quantum dots. The approach of the internal source has been extensively used over the past years to study the optical properties of photonic crystals [10]. For silicon-based materials, the quality factor measurement of nanocavities using the internal source is more cumbersome than for III-V materials because of the indirect band gaps of the materials and their poor emission efficiency when non radiative mechanisms are present. Despite this drawback, it has been shown that the photoluminescence of Ge/Si self-assembled islands embedded in nanocavities can be used to characterize the photonic crystals over a broad spectral range, from 1.2 to 1.6 $\mu m$, and this even at room temperature. Different type of defect-cavities or two-dimensional photonic crystals without defects have been investigated by this method [11, 12, 13]. The method requires to epitaxially grow a layer of Ge/Si self-assembled islands

before processing of the photonic crystals. Results obtained following the same approach have been reported by Xia *et al.* in 2006 with quality factors limited to 600 for H2 cavities [14].

Up to now, the silicon-based photonic crystal cavities investigated with an internal source did exhibit quality factors with values up to few thousands. The question arises whether the internal source technique can be used to study cavities on silicon with large quality factors. The case of silicon-based nanocavity is different from the case of III-V materials where the intrinsic absorption of the internal source like quantum dots limit the quality factors that can be measured [15]. Here the weak absorption of the indirect band gap Ge/Si self-assembled layer is not expected to limit the measurement for quality factors up to 100 000. Moreover, by opposition to III-V materials, the loss saturation effect and the increase in gain before entering the stimulated emission regime can not be achieved with standard silicon-based materials. In order to investigate the limits of the internal source for Si-based materials, we did focus on elongated L3 photonic crystal nanocavities with laterally shifted air hole positions. We show that the quality factor of these cavities markedly depend on the incident pump intensity. This dependence is a consequence of the free-carrier absorption which results from the photo-induced carriers. This dependence can be modeled by taking into account the different recombination pathways for the carriers. From the slope of the quality factor decrease *vs.* incident power, we get insight on the recombination mechanisms which limit the carrier density. We show that at room temperature the dynamics is governed by non radiative recombinations associated with surface recombinations. We show that the internal source technique becomes more and more difficult to use for cavities with very large quality factors since one has to reduce the incident excitation power below the microwatt in order to avoid the limitations due to free-carrier absorption.

## 2. Sample fabrication

The investigated structures were fabricated from a silicon-on-insulator substrate with a buried oxide thickness of 2 $\mu m$. The upper silicon crystalline layer was first thinned down to a thickness of 70 nm. This was followed by the epitaxial growth by chemical vapor deposition of silicon (60 nm), a single layer of Ge/Si self-assembled island and a silicon cap layer (130 nm thick). The total thickness of the layer above the buried oxide is $\simeq$ 260 nm. The sample was coated with a resist mask and photonic crystal patterns were designed by e-beam lithography. The photonic crystal area is 10 x 10 $\mu m^2$. Linear three-hole elongated defect cavities (L3) were obtained in triangular lattice patterns by omitting to drill three neighbouring holes along one direction. The holes were etched through the silicon matrix by inductively coupled reactive ion etching. The lattice period $a$ is 390 nm. The air hole radius is 0.295 a. The buried oxide was removed by selective wet etching using hydrofluoric acid resulting in the formation of air-bridge structures. The photoluminescence was excited with the 458 nm line of an argon ion laser. The reflection on the air-bridge is close to zero at this wavelength. The light was focused by a microscope objective with a 0.8 numerical aperture. The luminescence was collected with the same objective and analyzed with a 0.5 m focal length monochromator and a nitrogen-cooled multichannel InGaAs photodetector. Figure 1(a) shows a scanning electron micrograph image of the reference L3 cavity obtained after removing the buried oxide. Figure 1(b) shows an image of the same cavity with the edge air holes laterally shifted by a fraction of the lattice parameter (0.15 a). A close look at the image indicates that a small roughness is present on the unetched surface. This roughness stems from the buried islands and results from an incomplete smoothening of the surface during the island capping. By atomic force microscopy, a roughness of 18 nm (min-max) is measured for the surface covered by square-based pyramids. This roughness associated with a dot density of 3 x $10^9 cm^{-2}$ and a lateral size around 100 nm is a source of scattering for the optical modes.
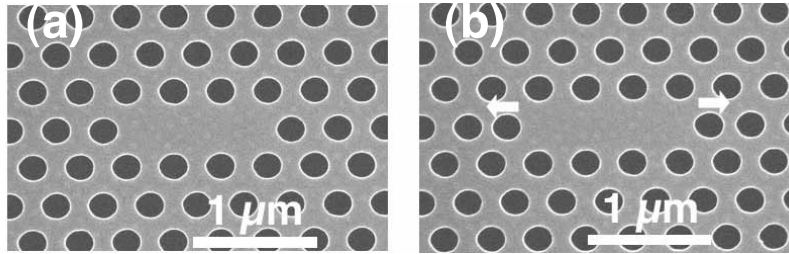
Fig. 1. (a) Scanning electron micrograph image of the L3 cavity. (b) Scanning electron micrograph image of the cavity with laterally shifted air holes (0.15 a).

## 3. Results

Figure 2 shows the room temperature photoluminescence of the unmodified three hole defect cavity (a) and the photoluminescence of the cavity with laterally shifted air holes (0.15 a) (b). The emission from the fundamental mode, which exhibits the smallest linewidth, is observed at $\lambda = 1551$ nm for the unmodified cavity and at $\lambda = 1559$ nm, corresponding to a normalized frequency u = a/$\lambda$ = 0.251 for the modified cavity. Additional modes are observed at shorter wavelengths. The observed modes can be classified according to their symmetry by respect to the symmetry plane in the middle of the slab. Even modes have an electric field in the middle of the slab polarized perpendicular to the holes while odd modes exhibit an electric field parallel to the holes. The fundamental mode has an even symmetry (TE-like) in this direction. The cavities are also symmetric along the $x$ and $y$ directions, the $x$ direction being along the three-hole missing line and the $y$ direction is perpendicular to it in the plane. The modes can be further classified by the symmetry of the electric field components along the $x$ and $y$ axis. The value of the quality factor of the fundamental mode is controlled by the components of the Fourier transform of the electric field within the light cone. An important feature is the amplitude ratio of the emission amplitude collected from the surface between the different optical modes of the defect cavity. Starting from the FDTD modeling, we have implemented a near-field to far-field conversion procedure [16] in order to calculate the theoretical radiation spectrum. In the modeling, dipole emitters with a broad spectral range and a density corresponding to the island density (30 per $\mu m^2$) were inserted in the middle of the silicon slab. We take into account the finite collection associated with a 0.8 numerical aperture. Figures 2(c) and (d) show the calculated radiation spectrum for the unmodified and the L3 0.15 a cavity respectively. A satisfying agreement with the experiment is obtained with the same number of modes or group of modes observed as predicted by the calculation. For the L3 0.15 a cavity the fundamental mode has an $E_x$ field with an odd parity along the $x$ and $y$ directions. The second mode which is observed around 1483 nm has an $E_x$ field parity even and odd along $x$ and $y$ directions respectively. It has a strong field overlap with the cavity edge along the $x$ direction and is very sensitive to the edge-hole displacement [17]. This mode is not observed in this energy range for the unmodified cavity. The next modes are a group of three modes around 1430 nm closely spaced in energy. The two dominant modes have an $E_x$ field with an even parity along the $x$ and $y$ directions. For the L3 0.15 a cavity, the difference of amplitude for the fundamental mode between experiments and modeling is attributed, as discussed below, to a lower experimental value of the quality factor as compared to modeling because of the free-carrier absorption and surface roughness (experimental Q value of 8 000 as compared to a calculated value of 47 500). The position of the islands and the polarization of the emission are also a source of discrepancy.

Figure 3 shows the dependence of the quality factor of the fundamental mode as a function of the symmetric displacement of the edge air holes. The displacement is given in fraction of
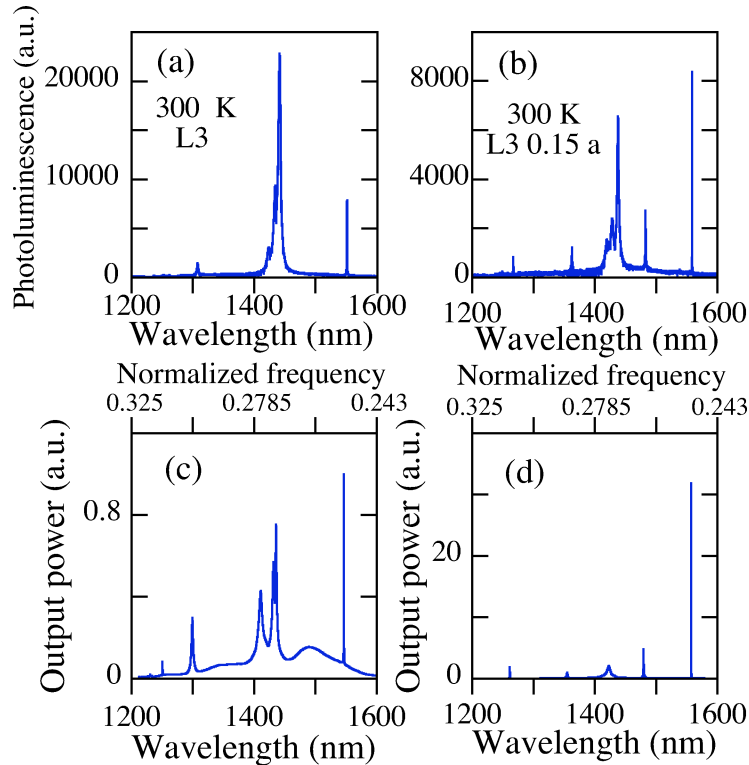
Fig. 2. a) Room temperature photoluminescence of the L3 cavity as shown in Fig. 1 (a). (b) Room temperature photoluminescence of an elongated three-hole defect cavity with laterally shifted air holes (0.15 a) as shown in Fig. 1 (b). The incident excitation power is 1 *mW*. (c) Calculated radiation spectrum of the L3 cavity obtained by 3D-FDTD simulation. (d) Calculated radiation spectrum of the L3 cavity with laterally shifted air holes (0.15 a) obtained by 3D-FDTD simulation.

the lattice parameter. The quality factor of the unmodified cavity is 5160. The quality factor increases as the edge air holes are symmetrically displaced. Experimentally, the value that can be measured is limited by the resolution of the spectrometer ($\sim$ 100 pm) corresponding to a quality factor value of $\sim$ 16 000. The values measured for the displacements 0.15 a and 0.175 a are thus limited by the spectrometer resolution. This dependence of Q *vs.* hole position was modeled by 3D-FDTD. The calculated quality factor of the unmodified cavity is 5020, in satisfying agreement with the experimental value. This value increases up to 77 000 for a lateral displacement of 0.175 a. The curve is strongly resonant, the increase of the quality factor being significant only for small variations around 0.175 a (full width at half maximum 0.05 a).

Figure 4 shows a comparison between the photoluminescence of the unprocessed sample and the photoluminescence of the fundamental mode with a lateral displacement of 0.15 a. An increase by a factor of 58 is observed for the emission amplitude of the fundamental defect cavity mode at 1559 nm. Many factors contribute to this enhancement. The main factor is obviously the change of the density of optical modes, the modification of radiation pattern and the change of extraction efficiency. The carrier diffusion and the local carrier density plays also an important role, and, as will be shown below, the recombination dynamics is governed by non radiative recombinations at the interface which in turn limits the internal radiative quantum efficiency. The position of the islands which varies from one cavity to another and their
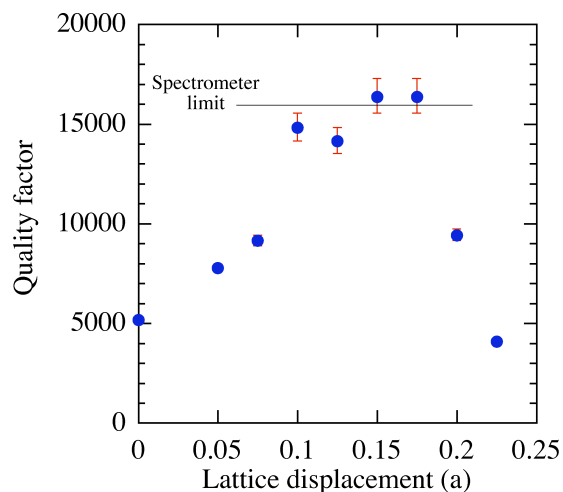
Fig. 3. Quality factor of the fundamental mode as a function of the symmetric lateral shift of the edge air holes of the L3 cavity. The spectrometer resolution limits the measurement at 16 000.

coupling to the electromagnetic field is also a parameter. The comparison between the photo-luminescence of the unprocessed sample, i.e. with the buried oxide and without air holes, and the photoluminescence of the defect cavity is thus not straightforward. It remains clear that the extraction efficiency of a defect cavity mode can be larger than that of a silicon slab [18]. The extraction efficiency of a thick slab of index $n$ towards the upper surface is $1/4n^2$. For a defect cavity mode, the extraction efficiency is given by the ratio $\frac{1/Q_z}{1/Q}$ where $Q_z$ is the quality factor corresponding to the coupling towards the surface and Q the total quality factor. Additionally, there might be an enhancement of the recombination rate by the Purcell effect. We note that the Purcell effect is dependent on the linewidth of the emitter and that usually this effect is smeared out at room temperature because of the large homogeneous broadening of the optical transitions. Moreover it is not obvious to obtain a signature of the Purcell modification of the recombination rate by investigating the *cw* dependence of the saturation intensity. Because of the large density of states of the Ge/Si self-assembled islands, an increase of the optical pump-ing intensity leads to a strong broadening of the room temperature photoluminescence of the islands and to a change of the overlap between the electron and hole wavefunctions which de-pend on the carrier density [19]. It is thus difficult to quantitatively relate a change of saturation intensity to the Purcell effect [20].

Figure 5 shows the dependence of the quality factor as a function of the incident excitation power. This dependence is shown for the unmodified three missing-hole cavity and for the cav-ity with a lateral displacement of 0.15 a. A strong decrease of the quality factor is observed as the incident power is increased, the quality factor can vary by more than one order of magni-tude for a two orders of magnitude change in the incident power. The intrinsic Q value of the defect cavity can thus only be obtained at low excitation power. This dependence is attributed to the free-carrier absorption associated with the photo-induced carriers generated by the 458 nm optical pumping. We have modeled this dependence by taking into account the different recombination mechanisms which control the carrier density. The dominant non-radiative re-combination rate is associated with recombination at the interfaces, the recombination at defect and impurities being assumed as negligible. A phenomenological value $1/\tau_{nr} = v_s/d$ where $v_s$ is the surface recombination velocity and d the slab thickness is considered. Radiative recom-
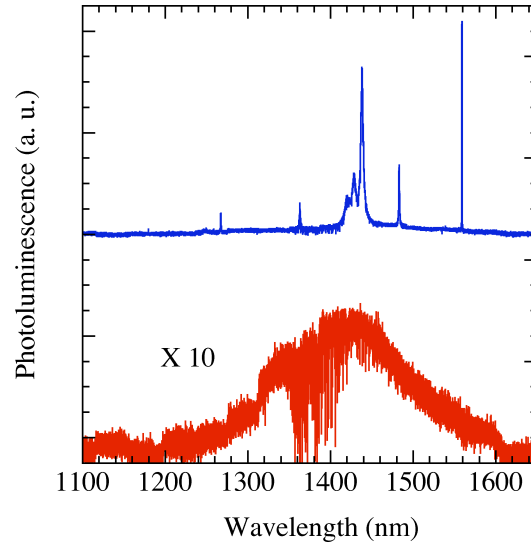
Fig. 4. Room temperature photoluminescence of the unprocessed sample (bottom figure) as compared to the photoluminescence of the L3 cavity with shifted air holes (0.15 a) (upper panel). The photoluminescence of the unprocessed sample has been multiplied by a factor of 10. The incident excitation power is 1 $mW$ for both measurements. The dominant peak corresponds to an amplitude of 100 cts/s.

binations and Auger-assisted recombinations proportional to $B N^2$ and $C N^3$ where $B$ and $C$ are the radiative and Auger-assisted recombination coefficients and N the three-dimensional carrier density were considered.

The rate equation for the carrier density is written as

$$\frac{dN}{dt} = \frac{\alpha I}{h\upsilon} - \frac{N}{\tau_{nr}} - BN^2 - CN^3 \tag{1}$$

where $\alpha$ is the absorption coefficient at 458 nm, I the incident intensity coupled to the slab, $h\upsilon$ the photon energy. All the parameters used in the modeling are summarized in table 1. The carrier density is obtained by solving Eq. (1) under steady state condition. The free-carrier absorption around 1.55 $\mu m$ is given by $\alpha = 1.45 \times 10^{-17}$ N(cm$^{-1}$) [21]. The quality factor of the cavity results from a balance between the intrinsic quality factor Q$_{int}$ and the quality factor given by the free-carrier absorption Q$_{abs} = \frac{2\pi n}{\alpha\lambda}$ following $1/Q = 1/Q_{int} + 1/Q_{abs}$. At high excitation power, the quality factor is limited by the free-carrier absorption and its value allows to estimate the carrier density. The slope of the Q factor *vs.* incident power is a direct indication of the dominant recombination mechanisms. The slope is more important if the carrier density is limited by the surface recombination instead of radiative recombinations or Auger-assisted recombinations. The full curves in Fig. 5 are the result of the modeling. It appears that the roll-off of the Q factor can *only* be described by a carrier density limited by non-radiative surface recombinations. If we consider the unmodified cavity, the best fit is obtained with a value of $\tau_{nr}$= 0.5 ns. This value controls the onset of the quality factor decrease. This short recombination time corresponds to a surface recombination velocity v$_s$ = 4.8 x $10^4$ $cm.s^{-1}$, which is in agreement with reported values of surface recombination of silicon [22]. This effective surface
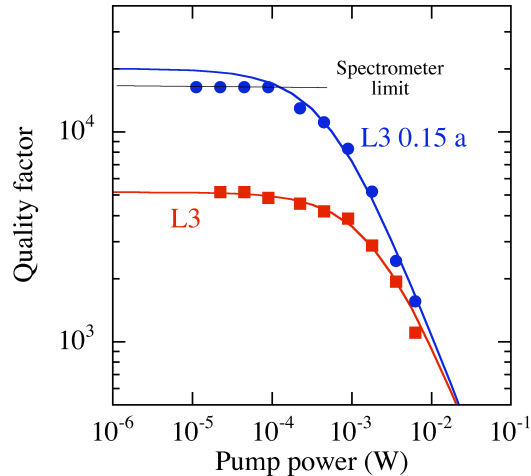
Fig. 5. Dependence of the quality factor of the fundamental mode as a function of the incident excitation power for the L3 cavity and the L3 cavity with shifted air holes (0.15 a). The full lines correspond to the numerical fit as described in the text, with an intrinsic quality factor of 5160 and 20000 respectively.

recombination velocity accounts for the increase of surface (membrane and sidewalls) due to the photonic crystal processing. The measurement of the quality factor of the cavities is thus a direct indication of the recombination mechanisms in these silicon-based two-dimensional photonic crystals which limit the carrier density. The quality factor becomes limited by Auger-assisted recombinations at powers larger than 100 mW. The fit of the experimental data of the modified L3 cavity corresponds to an intrinsic quality factor of 20 000. This value has to be compared to the theoretical value of 47 500. The difference is attributed to the scattering by the surface roughness induced by the presence of the buried islands. A way to circumvent this problem would be to planarize the surface before or after processing. This approach is however beyond the scope of this article. We emphasize that the measurement of the intrinsic quality factor of a cavity requires a weak incident excitation power, a parameter which has to be decreased when the quality factor increases. A cavity with a Q $\sim$100 000 requires an incident excitation power lower than the microwatt to be in the intrinsic regime. As we are dealing with indirect band gap materials with a weak radiative efficiency, it can rapidly become difficult to collect a significant number of photons within a reasonable time. The free-carrier absorption is thus the main limiting feature to characterize the silicon-based photonic crystals with an internal source. The modeling also provides an information on the radiative efficiency. The radiative efficiency increases up to 100 mW with a maximum around 2 x $10^{-4}$ and decreases at larger incident powers (onset of Auger-assisted recombinations). For a 10 mW incident excitation power, the radiative efficiency is around 2 x $10^{-5}$.

Figure 6 shows the dependence of the resonance wavelength as a function of the incident optical power. The measurement is performed with the L3 cavity and a lattice displacement of 0.15 a. The resonance wavelength remains constant up to 1 mW and starts to significantly increase at higher incident excitation powers. The relative variation $\triangle\lambda/\lambda \sim 0.008$ corresponds to a refractive index change $\sim$ 2.4 x $10^{-2}$. This red-shift of the emission is associated with a thermal effect and a non-linear increase of temperature corresponding to a change of refractive index. Two effects contribute mainly to this change of refractive index : the thermo-optic variation of the refraction coefficient and the change of index associated with the free-carriers. For a carrier density N$\sim$ 5 x $10^{18}$ cm$^{-3}$, obtained for a 6 mW incident excitation, the refractive index
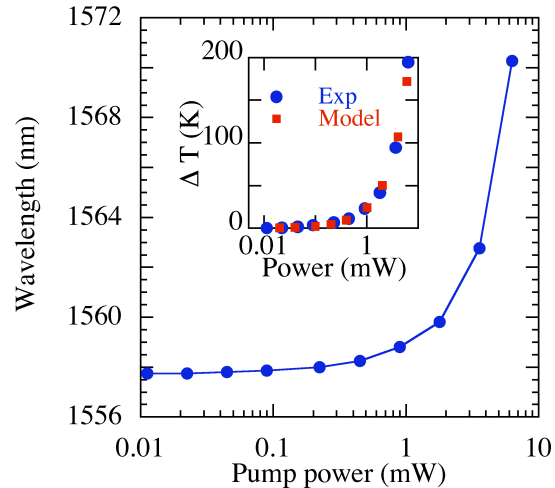
Fig. 6. Dependence of the resonance wavelength of the fundamental mode as a function of the incident excitation power. The full line is a guide to the eye. The inset shows a comparison between the measured temperature rise, deduced from the wavelength shift, and the calculated temperature rise.

change due to plasma effect, if we assume an equal concentration of electrons and holes, is $\sim$ - $(8.8 \times 10^{-22} \times N + 8.5 \times 10^{-18} \times N^{0.8}) \sim - 1.2 \times 10^{-2}$[21]. The temperature dependence of the refraction coefficient of silicon at room temperature is $1.85 \, 10^{-4}$/ K [23]. The wavelength shift corresponds thus to a temperature increase of $\sim$ 190 K in the air bridge at the highest excitation power. We have modeled the temperature rise solving the heat equation in the photonic crystal membrane surrounded by the silicon-on-insulator wafer. Finite element simulations were performed on bidimensional and axisymmetric bidimensional representation of the structure. The 260 nm membrane thickness, the 390 nm lattice period and the high carrier concentration act on the heat transport leading to the decrease of the effective thermal conductivity of the membrane compared to the Si bulk one [24]. A phenomenological temperature-dependent thermal conductivity $k(T) = 55(T/300)^{-0.85}$(W/m.K) was considered. It leads to an estimated temperature rise of about 210 K in the cavity for an incident power of 7 mW. The inset of Fig. 6 shows a comparison between the measured temperature rise and the calculated temperature rise. A good agreement is obtained between experiment and modeling. The lattice heating becomes quite important at large excitation powers. It can rapidly lead to a breakdown of the structure. The rapid change of wavelength of the defect-cavity mode is a signature of this thermal effect.

## 4. Discussion

### 4.1. Interest of the internal source technique

We have provided a detailed analysis of the internal source technique to characterize silicon-based photonic crystals. The internal source technique offers several advantages as compared to passive characterization techniques of photonic crystals : it allows to probe rapidly the optical properties of photonic crystals on a very large spectral range (roughly from 1100 to 1600 nm in this work) ; as compared to the passive technique, it provides simultaneously information on both TE and TM modes and it avoids to address the issue of coupling cavities with waveguides and coupling light efficiently in waveguides with reduced dimensions. It is well adapted to characterize small isolated patterns (typically 10 x 10 $\mu m^2$), not connected with long waveguides

to the sample cleaved edge. An example of such characterization in original 2,5 D photonic crystals is given in Ref. [13]. As compared to studies undertaken with III-V materials, the GeSi self-assembled islands are an indirect band gap material with an intrinsically reduced radiative efficiency. There is thus a trade-off between photon emission and optical losses induced by the interband optical pumping and the non-radiative recombinations. This work shows for the first time that even if the active material is an indirect band gap material, quality factors up to 20 000 can be measured at room temperature with this technique. This work also shows that since GeSi self-assembled islands can be in some cases significantly larger than III-V quantum dots, the smoothing of the surface by the capping layer can be incomplete and can limit the quality factor of the photonic crystal modes. A guidance for future developments in this field will be to perform a chemical mechanical polishing of the surface before processing the photonic crystals thus leading to larger quality factors. A strong dependence of the Q factor as a function of the incident power has been reported. It first indicates that small incident powers are required (below 100 $\mu W$) in order to measure Q factors larger than 10 000. It also indicates that free-carrier absorption induced by the interband optical pumping rapidly limits the quality factor, a situation quite different with the one observed with III-V photonic crystals. This point was not addressed in previous studies on silicon-based photonic crystals with GeSi self-assembled islands since the reported Q values were much smaller.

### 4.2. *Specific applications of the quantum dot-cavity system*

The power dependence of the quality factor indicates that the carrier density is limited by non-radiative recombinations and not by Auger-assisted recombinations. The knowledge of the non-radiative recombination time at the interfaces is important for future development of photonic crystal devices, in particular for those based on optical non linearities where large optical powers are required. The achievement of a net gain with a silicon Raman laser using slow modes of photonic crystal waveguides is limited by free-carrier absorption. The non-radiative recombination parameters obtained in this work will provide inputs for the modeling of future photonic crystal Raman lasers. These photonic crystal lasers are first developed on silicon-on-insulator substrates, i.e. without GeSi islands. However, the information obtained on the recombination velocity using the internal source technique is critical for designing and modeling the performances of these lasers. We are currently working in this direction. GeSi islands or GeSi quantum wells could provide a way to change the energy difference in the Raman process. Future work will also concentrate on the study of a single GeSi self-assembled quantum dot with reduced size embedded in a photonic crystal cavity with a small mode volume. An optimized enhanced coupling of the island with the cavity mode might provide a signature of Purcell enhanced optical recombination. Very weak excitation powers will be required for this study as evidenced by the results reported in this work. GeSi self-assembled islands embedded in photonic crystals are however not intended to provide an efficient optical light source with a large brightness.

### 5. Conclusion

In conclusion, we have investigated the measurement of quality factor of silicon-based photonic crystal nanocavities using an internal source technique at room temperature. This was illustrated for the case of L3 elongated cavities whose quality factors can be controlled by the lateral air hole positions. We have shown that the quality factor strongly depends on the incident excitation power. This dependence provides direct information on the carrier recombination dynamics. The carrier density was found to be controlled by non-radiative surface recombinations which lead to recombination lifetimes in the nanosecond range in these structures. Because of large free-carrier absorption, the internal source technique becomes difficult to implement to

study cavities with very high quality factors. The spectral position of the resonances are also dependent on the incident excitation power. A temperature increase $\sim 190$ K was experimentally observed, in agreement with two-dimensional thermal simulations.

**Acknowledgments**

Table 1

| Parameter | Value | unit | Reference |
|---|---|---|---|
| | | | |
| Absorption coefficient (458 nm) | 25 000 | $cm^{-1}$ | [25] |
| Radiative recombination coefficient B (300 K) | $4.73 \times 10^{-15}$ | $cm^3 s^{-1}$ | [26] |
| Auger recombination coefficient (300 K) | $10^{-31}$ | $cm^6 s^{-1}$ | [27] |
| Free-carrier absorption (1.55 $\mu m$) | $1.45\ 10^{-17} N$ | $cm^{-1}$ | [21] |
| $\partial n/\partial T$ (300 K) | $1.85 \times 10^{-4}$ | $K^{-1}$ | [23] |
| Thermal conductivity (300 K) | 55 | W/m.K | [24] |